Hindawi
Mathematical Problems in Engineering
Volume 2022, Article ID 4935623, 10 pages
https://doi.org/10.1155/2022/4935623

Research Article

Vibration of a Thermoelastic Microbeam due to the Thermoelectrical Effect of a Strip of Graphene

Ahmed N. M. Alahmadi

Electrical Engineering Department, Umm Al-Qura University, Makkah 21955, Saudi Arabia

Correspondence should be addressed to Ahmed N. M. Alahmadi; anmahmadi@uqu.edu.sa

Received 22 January 2022; Accepted 15 March 2022; Published 6 April 2022

Academic Editor: Georgios I. Giannopoulos

In this work, an analysis of thermoelastic, homogeneous, and isotropic microbeams was conducted in the context of the non-Fourier heat conduction law. The first end of the microbeam was based on a graphene strip, which was connected to an electrical voltage source. Under simple boundary conditions maintained by fixed side ratios, the Lord–Shulman model of generalized thermoelasticity was applied. The microbeam was thermally loaded with a heat source due to the thermal effect of the electrical current that ran through the strip of graphene. Laplace transformation of the time variable was utilized to solve controlled differential equations. All the solutions were found in the Laplace transform domain. Tzou's approximation approach, which relies on an iteration formula, was used to numerically calculate the Laplace transform inversions. For different values of the electrical voltage and the resistance of the graphene strip, different graphs were used to show the numerical results. The electrical voltage and the electrical resistance were reported to have significant influences on all the studied functions of the microbeam. Thus, controlling a microbeam's vibration and energy could be accomplished by tuning the electrical resistance and applied voltage.

1. Introduction

Fourier's law of heat conduction is the basis for linked thermoelasticity, which is a type of heat conduction based on two partial differential equations, one for motion and another for conserving energy [1–3]. In the case of an isotropic body, Lord and Shulman amended Fourier's rule of heat conduction by incorporating the relaxation time into the equation [4]. Specifically, Cattaneo's heat conduction, which is also known as non-Fourier heat conduction law, has been modified to incorporate both the heat flux and its time derivative, and it has been considered as a substitute for the standard Fourier's law of heat conduction. Accordingly, there are no infinite propagation problems, as the heat equation is hyperbolic [5–9].

The most fundamental type of microbeam resonator is the vibration microbeam. There have been numerous studies on the vibration and heat transfer processes of microbeams [10–19]. The Green functions and their properties were utilized by Kidawa-Kulka to investigate the transversal vibrations caused by a moving heat source and the effects of internal and external dampening [15]. Manolis and Beskos used a computational analysis approach to evaluate the elastic dynamic response of a beam structure to heat loading [16].

The investigation of visco-thermoelastic materials, which are known to often have relaxation properties, has become increasingly important in mechanics. Biot has written about the theory of visco-thermoelasticity, as well as vibrational principles in thermodynamics, among other things [20, 21]. Drozdov developed a constitutive model of the visco-thermoelasticity behaviour of polymers when they are subjected to finite strains [22]. Using a new visco-thermoelasticity model for isotropic media, Ezzat and El-Karamany investigated the consequences of relaxation on the volume features of viscoelastic materials to study the transversal vibrations caused by a moving heat source and the effects of internal and external dampening [23]. A numerical approach for wave simulations in elastic media was developed by Carcione et al., and it was based on the Kelvin–Voigt

mechanical model [24]. The resonance of a microscale visco-thermoelastic beam and its transverse vibrations were studied by Grover [25–27]. In addition, an analysis applying closed-form equations for thermoelastic thin beam transverse vibrations with micro or nanoscale vacancies was carried out by Sharma and Grover [10]. Using a dual phase-lagging model, Grover and Seth investigated visco-thermoelastic microscale beam resonators [28].

Since the ground-breaking observations of Novoselov et al., graphene has continued to pique the interest of scientists around the world [29]. The electronic properties of graphene as a single-layer material are intriguing and include ballistic transport, a quantum Hall effect at ambient temperature, and a size-dependent band gap, all of which have the potential to enable new types of microscale electronic devices and sensors [30].

In this work, for the first time, an analysis for thermoelastic, homogeneous, and isotropic microbeams was conducted in the context of the non-Fourier heat conduction law when the first end of the microbeam was based on a graphene strip connected to an electrical voltage. Because of the thermal effect of the electrical current running on the graphene strip, the microbeam was thermally loaded with a heat source. The microbeam was electrically isolated using an electrical isolator with high thermal conductivity, as shown in Figure 1.

2. Problem Formulation

For a narrow thermoelastic microbeam with length of $\ell\,(0 \le x \le \ell)$, a width of $b\,(-b/2 \le y \le b/2)$, and a thickness of $h\,(-h/2 \le z \le h/2)$, we considered the flexural deflections to be very small.

As shown in Figure 1, the x, y, and z axes of the beam are specified as the longitudinal, width, and thickness directions of the beam, respectively.

We considered there was no damping and no stress or strain, and that the reference temperature T_0 was constantly in an equilibrium condition for the microbeam [5]. At first, while any plane's cross section is bent perpendicular to a beam's axis (the "neutral surface"), it will remain perpendicular to the beam's axis and plane, as determined by the Euler–Bernoulli equation [25]. Consequently, displacement elements are formed [25, 27, 28, 31]:

$$u(x,y,z,t) = -z\frac{\partial w(x,t)}{\partial x}, v(x,y,z,t) = 0, w(x,y,z,t) = w(x,t). \tag{1}$$

The flexural moment of the cross section and the equation of motion are given by [25, 27, 28, 31]

$$M(x,t) = (\lambda + 2\mu) I \frac{\partial^2 w(x,t)}{\partial x^2} + \beta M_T(x,t). \tag{2}$$

The above equation contains the thermal moment M_T about the beam axis, the elastic term due to the vibration of the beam $\partial^2 w(x,t)/\partial x^2$, and the total flexural moment of the cross section of the beam, where the equation of motion is in the following form [25, 27, 28, 31]:

$$\frac{\partial^2 M(x,t)}{\partial x^2} + \rho A \frac{\partial^2 w(x,t)}{\partial t^2} = 0. \tag{3}$$

The thermal moment of the microbeam's x-axis, M_T, is calculated using [25–28, 31, 32]

$$M_T(x,t) = b\int_{-h/2}^{h/2} T(x,z,t) z \mathrm{d}z, \tag{4}$$

where $I = bh^3/12$ denotes the cross-sectional moment of inertia about the x-axis, λ and μ are the elastic constants, ρ is the density, A is the cross-sectional area, and $\beta = (3\lambda + 2\mu)\alpha_T$.

Therefore, the equation of motion that results in lateral vibrations of the microbeam due to thermally induced vibrations has the following form [25]:

$$(\lambda + 2\mu) I \frac{\partial^4 w(x,t)}{\partial x^4} + \rho A \frac{\partial^2 w(x,t)}{\partial t^2} + \beta \frac{\partial^2 M_T(x,t)}{\partial x^2} = 0. \tag{5}$$

The cross-sectional area is given by $A = hb$.

The heat conduction equation of Lord–Shulman has the following form [25]:

$$\frac{\partial^2 T(x,z,t)}{\partial x^2} + \frac{\partial^2 T(x,z,t)}{\partial z^2} = \left(\frac{\partial}{\partial t} + \tau \frac{\partial^2}{\partial t^2}\right)\left(\frac{\rho C_v}{K} T(x,z,t) + \frac{\beta T_0}{K} e(x,z,t)\right) - \left(1 + \tau \frac{\partial}{\partial t}\right)\frac{Q(x,z,t)}{K}, \tag{6}$$

where τ is the thermal relaxation time parameter, C_v is the specific heat at a constant strain, Q is the heat source, and K is the thermal conductivity.

The cubical dilatation (volumetric strain) has the following form:

$$e(x,z,t) = \frac{\partial u(x,z,t)}{\partial x} + \frac{\partial v(x,z,t)}{\partial y} + \frac{\partial w(x,z,t)}{\partial z}. \tag{7}$$

Thus, from (1), we have

$$e(x,z,t) = -z\frac{\partial^2 w(x,t)}{\partial x^2}. \tag{8}$$

We then obtain

$$\sigma_{xx}(x,z,t) = (\lambda + 2\mu) e(x,z,t) - \beta\theta(x,z,t). \tag{9}$$

Since there is no heat transfer at the upper and bottom sides of the beam, $\partial T(x,z,t)/\partial z|_{z=\pm h/2} = 0$. As a result, we may assume that the temperature relies on the function of $\sin(pz)$ in the direction of the beam's thickness, where $p = \pi/h$, which yields [33]

$$\theta(x,z,t) = T(x,z,t) - T_0 = \vartheta(x,t)\sin(pz), \tag{10}$$

$$Q(x,z,t) = q(x,t)\sin(pz). \tag{11}$$

The temperature increment is maintained at $\theta(x,z,t)$.

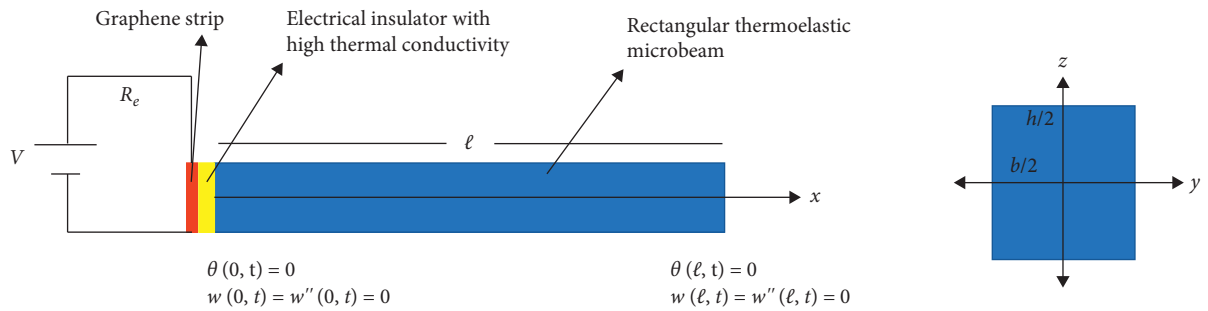

FIGURE 1: Rectangular thermoelastic microbeam based on a strip of graphene.

As a result of incorporating (4), (5), and (10), the following result was obtained:

$$\frac{\partial^4 w(x,t)}{\partial x^4} + \frac{12\rho}{h^2(\lambda+2\mu)}\frac{\partial^2 w(x,t)}{\partial t^2} + \frac{12\beta}{h^3(\lambda+2\mu)}\frac{\partial^2 \vartheta(x,t)}{\partial x^2}\int_{-\frac{h}{2}}^{\frac{h}{2}} \sin(pz)z\ dz = 0. \tag{12}$$

By using (6) and (10), we obtained

$$\left(\frac{\partial^2 \vartheta(x,t)}{\partial x^2} - p^2\vartheta(x,t)\right)\sin(pz) = \left(\frac{\partial}{\partial t} + \tau\frac{\partial^2}{\partial t^2}\right)\left(\varepsilon\vartheta(x,t)\sin(pz) + \frac{T_0\beta}{K}z\frac{\partial^2 w(x,t)}{\partial x^2}\right) - \left(1+\tau\frac{\partial}{\partial t}\right)\frac{q(x,t)}{K}\sin(pz), \tag{13}$$

where $\varepsilon = \rho C_v/K$.

(12) has the following form when the integrations have been concluded:

$$\frac{\partial^4 w(x,t)}{\partial x^4} + \frac{12\rho}{h^2(\lambda+2\mu)}\ddot{w}(x,t) + \frac{24\beta}{h\pi^2(\lambda+2\mu)}\frac{\partial^2 \vartheta(x,t)}{\partial x^2} = 0. \tag{14}$$

After multiplying both sides by z and integrating z from $(-h/2)to(h/2)$ in (13), we obtained

$$\frac{\partial^2 \vartheta(x,t)}{\partial x^2} - p^2\vartheta(x,t) = \left(\frac{\partial}{\partial t} + \tau\frac{\partial^2}{\partial t^2}\right)\left(\varepsilon\vartheta(x,t) - \frac{T_0 h\pi^2\beta}{24K}\frac{\partial^2 w(x,t)}{\partial x^2}\right) - \left(1+\tau\frac{\partial}{\partial t}\right)\frac{q(x,t)}{K}. \tag{15}$$

(9) takes the following form:

$$\sigma_{xx} = (\lambda+2\mu)e - \beta\vartheta\ \sin(pz). \tag{16}$$

The non-dimensional variables specified below were utilized [21]:

$$(x', w', h') = \varepsilon c_0(x, w, h),\ (t', \tau') = \varepsilon c_0^2(t, \tau),\ \sigma' = \frac{\sigma}{\lambda+2\mu},\ \vartheta' = \frac{\vartheta}{T_0},\ q' = \frac{q}{T_0 K\varepsilon^2 c_0^2},\ c_0^2 = \frac{\lambda+2\mu}{\rho}. \tag{17}$$

Following that, we obtained

$$\frac{\partial^4 w(x,t)}{\partial x^4} + \varepsilon_1 \ddot{w}(x,t) + \varepsilon_2 \frac{\partial^2 \vartheta(x,t)}{\partial x^2} = 0, \tag{18}$$

$$\frac{\partial^2 \vartheta(x,t)}{\partial x^2} - \varepsilon_3 \vartheta(x,t) = \left(\frac{\partial}{\partial t} + \tau \frac{\partial^2}{\partial t^2}\right)\left(\vartheta(x,t) - \varepsilon_4 \frac{\partial^2 w(x,t)}{\partial x^2}\right) - \left(1 + \tau \frac{\partial}{\partial t}\right) q(x,t), \tag{19}$$

$$\sigma_{xx}(x,z,t) = e(x,z,t) - \varepsilon_5 \vartheta(x,t) \sin(pz), \tag{20}$$

where $\varepsilon_1 = 12/h^2, \varepsilon_2 = 24\beta T_0/h\pi^2(\lambda + 2\mu), \varepsilon_3 = p^2$, $\varepsilon_4 = \pi^2 h\beta/24K\varepsilon$, and $\varepsilon_5 = \beta T_0/(\lambda + 2\mu)$ (the primes have been dropped for convenience).

Laplace transform with the following definition was applied:

$$\overline{f}(x,s) = \int_0^\infty f(x,t) e^{-st} dt\ . \tag{21}$$

The Laplace transform's inverse is expressed as [34]

$$L^{-1}(\overline{f}(s)) = f(t) \approx \frac{e^{\kappa t}}{t}\left[\frac{1}{2}\overline{f}(\kappa) + \mathrm{Re}\sum_{n=1}^{N} (-1)^n \overline{f}\left(\kappa + \frac{in\pi}{t}\right)\right]. \tag{22}$$

Many investigations have verified that the value of the parameter κ would fit the relationship $\kappa t \approx 4.7$ [34], to ensure a faster convergence, where "Re" denotes the real elements and "i" denotes the imaginary number unit.

Equations (18)–(20) then take the following forms:

$$\frac{d^4 \overline{w}}{dx^4} + \varepsilon_1 s^2 \overline{w} + \varepsilon_2 \frac{d^2 \overline{\vartheta}}{dx^2} = 0,$$

$$\frac{d^2 \overline{\vartheta}}{dx^2} - \varepsilon_3 \overline{\vartheta} = \left(s + \tau s^2\right)\left(\overline{\vartheta} - \varepsilon_4 \frac{d^2 \overline{w}}{dx^2}\right) - (1 + \tau s)\overline{q},$$

$$\overline{\sigma}_{xx} = \overline{e} - \varepsilon_5 \overline{\vartheta} \sin(pz), \tag{23}$$

$$\overline{e} = -z \frac{d^2 \overline{w}}{dx^2}. \tag{24}$$

Consider an electrical current connected to the strip of graphene, which has an electrical resistance $R_e(\Omega)$, where the graphene strip is attached at the starting end of the microbeam, as shown in Figure 1. The beam is subjected to specific heating resulting from the thermal effect caused by the connection of the graphene strip to an electric voltage source (Joule's equation of electrical heating) $V(V)$.

The heat flux is then calculated using Joule's equation of electrical heating as follows [29]:

$$q(x,t) = \frac{V^2}{R_e} t, \tag{25}$$

where V is the voltage and R_e is the electrical resistance.

Then, after using the Laplace transform, we have

$$\overline{q} = \frac{V^2}{R_e s^2}, \tag{26}$$

which gives

$$\frac{d^2 \overline{\vartheta}}{dx^2} - \varepsilon_3 \overline{\vartheta} = \left(s + \tau s^2\right)\left(\overline{\vartheta} - \varepsilon_4 \frac{d^2 \overline{w}}{dx^2}\right) - \frac{(1 + \tau s)V^2}{s^2 R_e}. \tag{27}$$

We can then rewrite equations (23) and (24) in the following forms:

$$\left(D^4 + \varepsilon_1 s^2\right)\overline{w} + \varepsilon_2 D^2 \overline{\vartheta} = 0, \tag{28}$$

$$\varepsilon_4\left(s + \tau s^2\right) D^2 \overline{w} + \left(D^2 - \left(\varepsilon_3 + s + \tau s^2\right)\right)\overline{\vartheta} = -\frac{(1 + \tau s)V^2}{s^2 R_e}, \tag{29}$$

where $D^r = d^r/dx^r$.

By elimination between (28) and (29), we obtain

$$\left\{D^6 - LD^4 + MD^2 - N\right\}\overline{w} = 0, \tag{30}$$

$$\left\{D^6 - LD^4 + MD^2 - N\right\}\overline{\vartheta} = -\psi, \tag{31}$$

where $L = \varepsilon_2\varepsilon_4(s + \tau s^2) + (\varepsilon_3 + s + \tau s^2), M = \varepsilon_1 s^2, N = \varepsilon_1 s^2(\varepsilon_3 + s + \tau s^2)$, and $\psi = \varepsilon_1(1 + \tau s)V^2/R_e$.

The general solution of (30) is as follows:

$$\overline{w} = \sum_{j=1}^{3} A_j \sin h\left(k_j(\ell - x)\right). \tag{32}$$

The general solution of equation (33) is as follows:

$$\overline{\vartheta} = \frac{\psi}{N} + \sum_{j=1}^{3} B_j \sin h\left(k_j(\ell - x)\right). \tag{33}$$

To obtain the relationship between the parameters A_j and B_j, we use the relationship in (28), which gives

$$\left(K_j^4 + \varepsilon_1 s^2\right)A_j + \varepsilon_2 K_j^2 B_j = 0,\ j = 1,2,3. \tag{34}$$

We then have

$$\overline{\vartheta} = \frac{\psi}{N} - \frac{1}{\varepsilon_2}\sum_{j=1}^{3} \frac{\left(K_j^4 + \varepsilon_1 s^2\right)}{K_j^2} A_j \sin h\left(k_j(\ell - x)\right). \tag{35}$$

The boundary conditions were

$$\sum_{j=1}^{3} A_j \sinh\left(k_j \ell\right) = 0, \tag{36}$$

$$\sum_{j=1}^{3} k_j^2 A_j \sinh\left(k_j \ell\right) = 0, \tag{37}$$

$$\sum_{j=1}^{3} \frac{\left(K_j^4 + \varepsilon_1 s^2\right)}{K_j^2} A_j \sinh\left(k_j \ell\right) = \frac{\varepsilon_2 \psi}{N}. \tag{38}$$

By solving equations (38)–(40), we obtained the parameters A_1, A_2, A_3 as follows.

$A_1 = \varepsilon_2\psi/\varepsilon_1 s^2 (k_1^2 - k_2^2)(k_1^2 - k_3^2)\sinh(k_1\ell)$, $A_2 = \varepsilon_2\psi/\varepsilon_1 s^2 (k_2^2 - k_1^2)(k_2^2 - k_3^2)\sinh(k_2\ell)$, and $A_3 = \varepsilon_2\psi/\varepsilon_1 s^2 (k_3^2 - k_1^2)(k_3^2 - k_2^2)\sinh(k_3\ell)$.

This completes the solution of the Laplace transform domain.

The lateral deflection function is as follows:

$$\overline{w}(x,s) = \frac{\varepsilon_2\psi}{\varepsilon_1 s^2} \left[\begin{array}{c} \dfrac{\sinh\left(k_1(\ell - x)\right)}{\left(k_1^2 - k_2^2\right)\left(k_1^2 - k_3^2\right)\sinh\left(k_1\ell\right)} + \\ \dfrac{\sinh\left(k_2(\ell - x)\right)}{\left(k_2^2 - k_1^2\right)\left(k_2^2 - k_3^2\right)\sinh\left(k_2\ell\right)} + \\ \dfrac{\sinh\left(k_3(\ell - x)\right)}{\left(k_3^2 - k_1^2\right)\left(k_3^2 - k_2^2\right)\sinh\left(k_3\ell\right)} \end{array} \right]. \tag{39}$$

The temperature increment function is as follows:

$$\overline{\theta}(x,s) = \frac{\psi \sin(pz)}{\varepsilon_1 s^2\left(\varepsilon_3 + s + \tau s^2\right)} + \frac{\varepsilon_2 \psi \sin(pz)}{\varepsilon_1 s^2} \left[\begin{array}{c} \dfrac{\left(K_1^4 + \varepsilon_1 s^2\right)\sinh\left(k_1(\ell - x)\right)}{K_1^2\left(k_1^2 - k_2^2\right)\left(k_1^2 - k_3^2\right)\sinh\left(k_1\ell\right)} + \\ \dfrac{\left(K_2^4 + \varepsilon_1 s^2\right)\sinh\left(k_2(\ell - x)\right)}{K_2^2\left(k_2^2 - k_1^2\right)\left(k_2^2 - k_3^2\right)\sinh\left(k_2\ell\right)} + \\ \dfrac{\left(K_3^4 + \varepsilon_1 s^2\right)\sinh\left(k_3(\ell - x)\right)}{K_3^2\left(k_3^2 - k_1^2\right)\left(k_3^2 - k_2^2\right)\sinh\left(k_3\ell\right)} \end{array} \right]. \tag{40}$$

From (24) and (39), we obtained the deformation in the following form:

$$e(x,z,s) = \frac{-z\varepsilon_2\psi}{\varepsilon_1 s^2} \left[\begin{array}{c} \dfrac{k_1^2 \sinh\left(k_1(\ell - x)\right)}{\left(k_1^2 - k_2^2\right)\left(k_1^2 - k_3^2\right)\sinh\left(k_1\ell\right)} + \\ \dfrac{k_2^2 \sinh\left(k_2(\ell - x)\right)}{\left(k_2^2 - k_1^2\right)\left(k_2^2 - k_3^2\right)\sinh\left(k_2\ell\right)} + \\ \dfrac{k_3^2 \sinh\left(k_3(\ell - x)\right)}{\left(k_3^2 - k_1^2\right)\left(k_3^2 - k_2^2\right)\sinh\left(k_3\ell\right)} \end{array} \right]. \tag{41}$$

The strain-energy density function through the microbeam is given by [35–37]

$$\varpi(x,z,t) = \sum_{i,j}^{3} \frac{1}{2}\sigma_{ij}(x,z,t)e_{ij}(x,z,t) = \frac{1}{2}\sigma(x,z,t)e(x,z,t). \tag{42}$$

3. Numerical Results and Discussion

As copper is a thermoelastic material, the following physical constants were utilized to describe the material [27, 38–40]: $\rho = 8954\,kg\mathrm{m}^{-3}$, $\alpha_T = 1.78\,(10)^{-5}\,\mathrm{K}^{-1}$, $k = 386\,Wm^{-1}\mathrm{K}^{-1}$, $\lambda = 77.6 \times 10^9\,\mathrm{Nm}^{-2}$, $\tau_0 = 4.32 \times 10^{-13}\mathrm{s}$, $C_v = 383.1\,Jkg^{-1}\,\mathrm{K}^{-1}$, $T_0 = 300\,\mathrm{K}$, and $\mu = 38.6 \times 10^9\,\mathrm{Nm}^{-2}$.

The resistance of the graphene at the microscale has the value $R_e = 500\,\Omega$ [30].

The microbeam's aspect ratios were set at $\ell/h = 8$ and $b = h/2$. However, a microbeam length range of $\ell(1 - 100) \times 10^{-6}\mathrm{m}$ was used, while the original time t and the relaxation time τ_0 were on the scale of 10^{-12} and 10^{-14} s, respectively.

The dimensionless variables for microbeam length $\ell = 1.0$, $\theta_0 = 1.0$, $z = h/4$, and $t = 1.0$ were used to generate the figures.

The numerical results of the problem have been illustrated in two groups of figures. The first group shows the distributions of the vibration (lateral deflection), cubical deformation, temperature increment, stress, and strain-energy density when the electrical resistance of strip of the graphene was constant and had the value $R_e = 500\,\Omega$ with three different values of the electrical voltage $V = (10, 11, 12)\mathrm{V}$. The second group represents the distributions of the same functions when the value of the electrical voltage was constant at a value of $V = 10\mathrm{V}$ but with three different values of electrical resistance, $R_e = (500, 600, 700)\Omega$.

Figure 2 shows that the value of the electrical voltage had a considerable impact on the distributions of vibration (lateral deflection), temperature increment, cubical

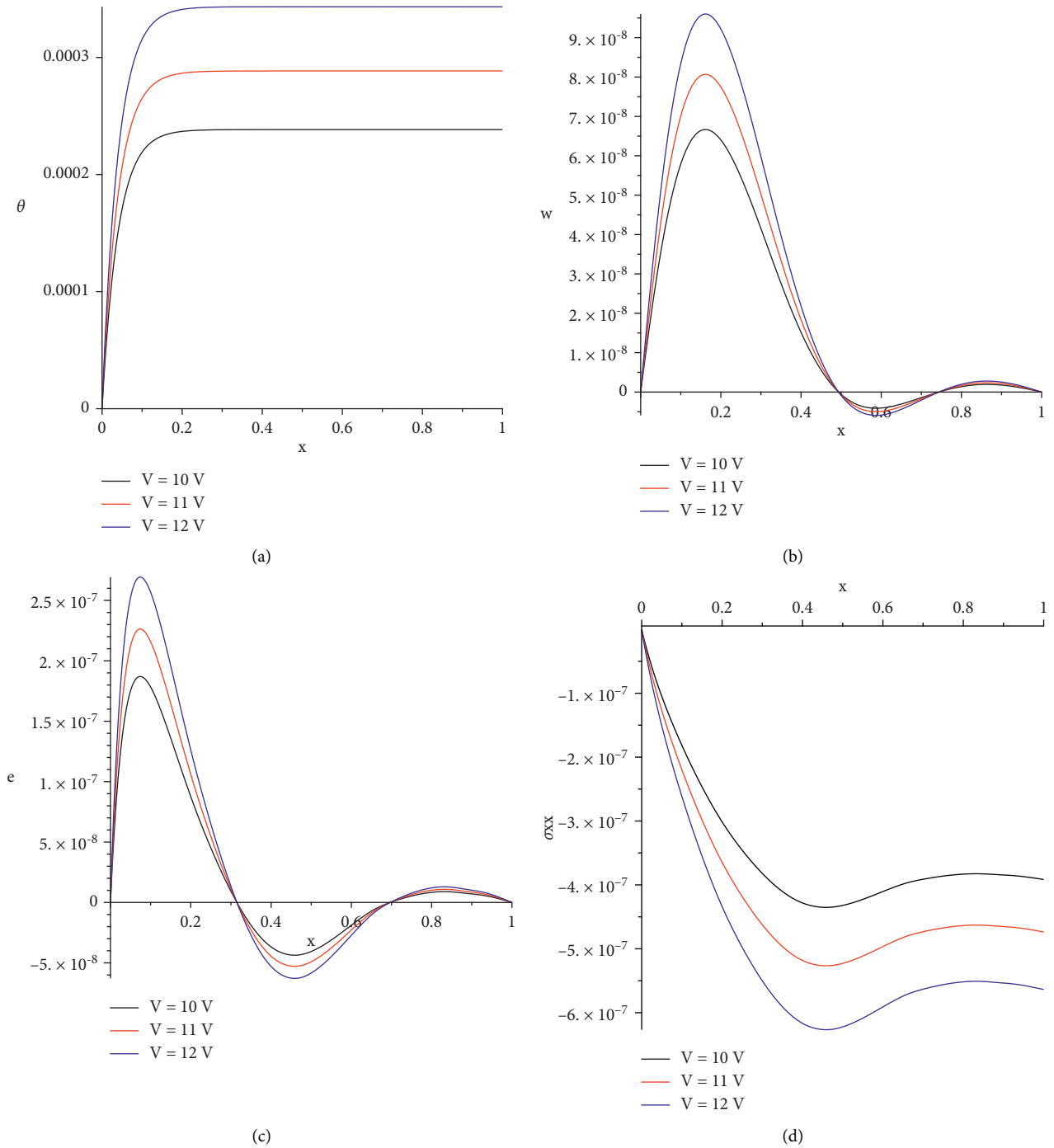

Figure 2: Continued.

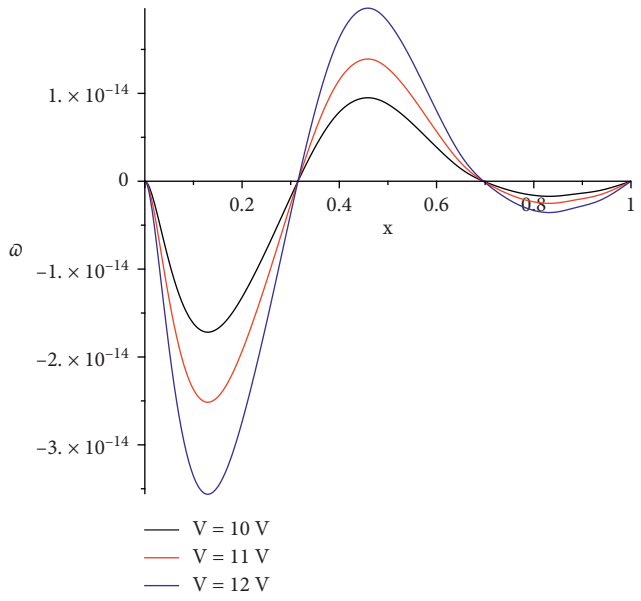

(e)

Figure 2: (a) The distribution of the temperature increment with different values of voltage. (b) The distribution of the vibration with different values of voltage. (c) The distribution of the cubical deformation with different values of voltage. (d) The distribution of the stress with different values of voltage. (e) The distribution of strain-energy density with different values of voltage.

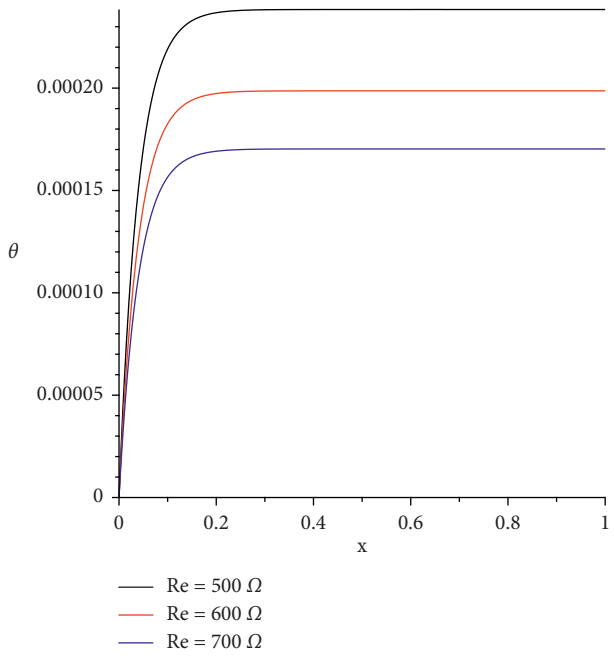

(a)

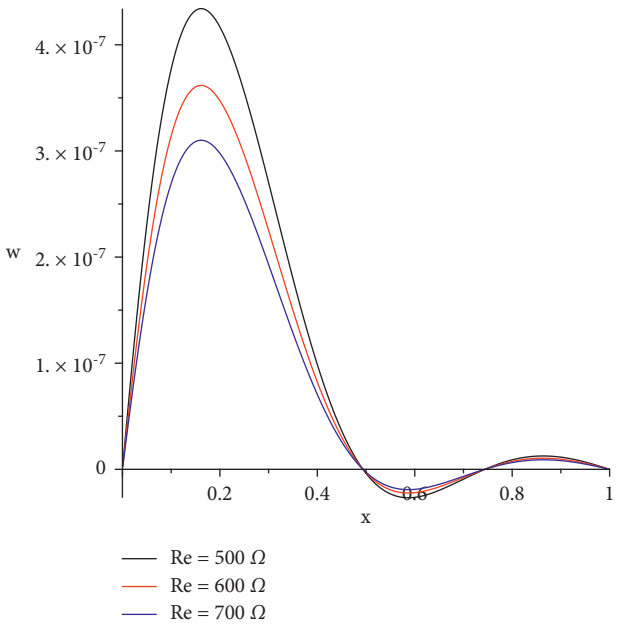

(b)

Figure 3: Continued.

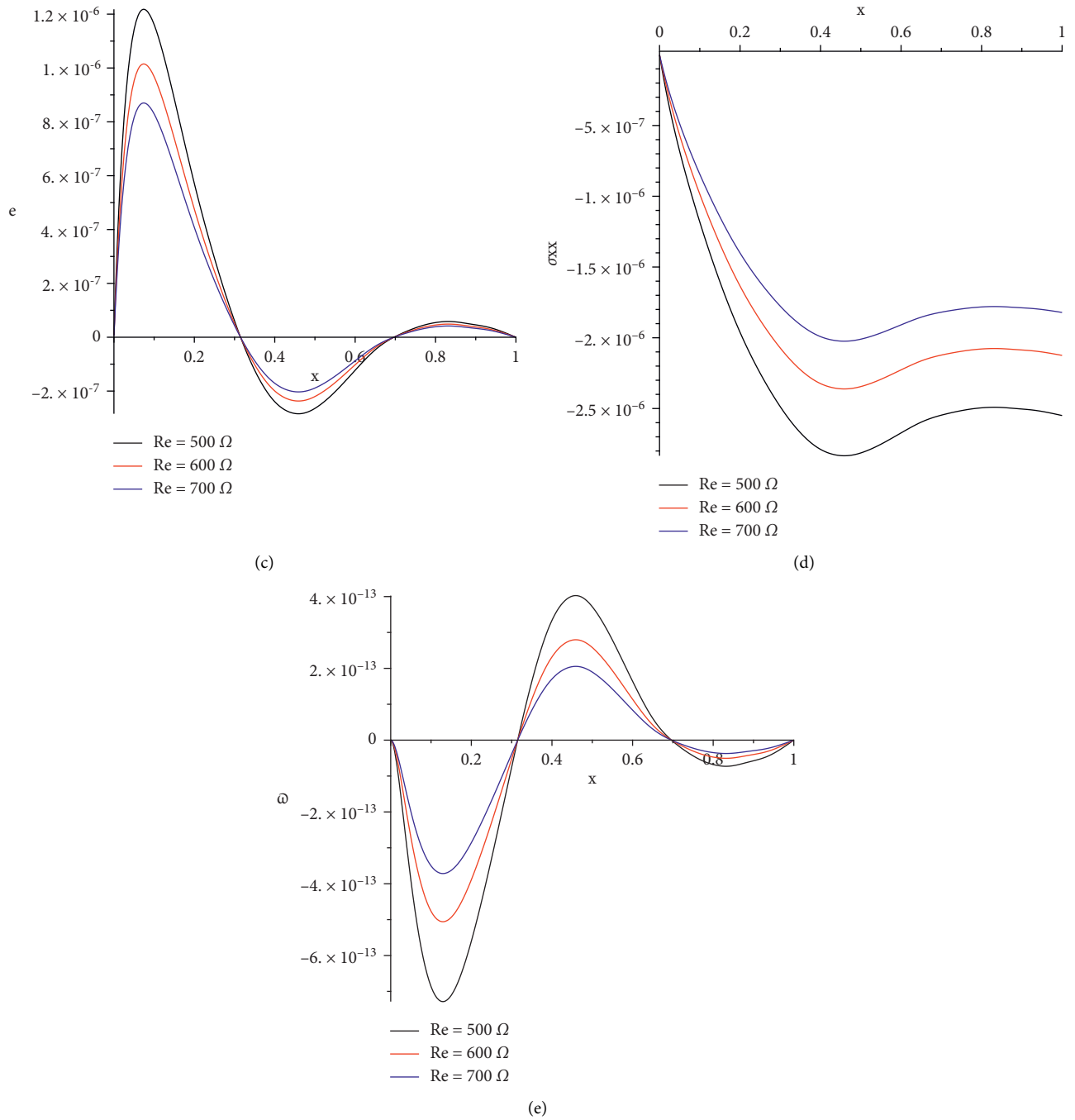

Figure 3: (a) The distribution of the temperature increment with different values of resistance. (b) The distribution of the vibration with different values of resistance. (c) The distribution of the cubical deformation with different values of resistance. (d) The distribution of the stress with different values of resistance. (e) The distribution of the strain-energy density with different values of resistance.

deformation, stress, and strain-energy density. An increase in the value of the electrical voltage led to an increase in the temperature increment and the absolute values of vibration (lateral deflection), cubical deformation, stress, and strain-energy density.

In Figure 2(a), the three curves show that the value of the temperature increment increased sharply for a distance of not more than 0.1 due to the thermoelectrical effect at this end; then, the curves entered a stage of stability until the end but with different values, depending on the voltage value. In Figures 2(b), 2(c), and 2(e), the value of the peak point in each curve increased as the value of the voltage increased. Along the x-axis, the values of the peak points decreased as the distance x increased. In Figure 2(d), each curve of the stress curves had only one peak point, and their absolute values increased when the voltage value increased.

The distributions of temperature increment, vibration (lateral deflection), cubical deformation, stress, and strain-energy density were all significantly affected by the electrical resistance value, as shown in Figure 3. The temperature increment and the absolute values of vibration (lateral deflection), cubical deformation, stress, and strain-energy density decreased with an increase in the electrical resistance.

Figure 3(a) shows that the value of temperature increment increased sharply for a distance of not more than 0.1 due to the thermoelectrical effect at this end; then, the curves progressed to the stage of stability until the end, but with different values depending on the value of electrical resistance. Figures 3(b), 3(c), and 3(e) show that the value of the peak point in each of the three curves decreased as the value of electrical resistance increased. The values of the peak points decreased with an increase in the distance x along the x-axis. Figure 3(d) shows that the stress curves had one peak point, and their absolute values reduced as the electrical resistance increased.

Thus, we can say that the electrical resistance could be used to tune the vibration as well as the energy which has been generated along the microbeam.

4. Conclusions

Non-Fourier heat conduction was used to analyse thermoelastic microbeams in this study. An electrical voltage source was connected to the graphene strip at the initial end of the microbeam. The Lord–Shulman model of generalized thermoelasticity was applied. As a result of the electrical current running in a strip of graphene, the microbeam was thermally loaded.

In all the functions studied, electrical voltage and electrical resistance were found to have a significant impact. The temperature increment and the absolute values of the vibration (lateral deflection), cubical deformation, stress, and strain-energy density increased as the electrical voltage increased. With increasing electrical resistance, the temperature and the absolute values of vibration (lateral deflection), cubical deformation, stress, and strain-energy density increased. Thus, the electrical voltage and resistance of the graphene strip might be utilized as a tuner to control the vibration and energy of a microbeam.

In general, the results agree with the results in other papers such as references [10, 13, 16, 25, 28, 35]. In the future work, electrical voltage as a heat source will be applied on different types of beams and in the context of different types of heat conduction laws.

Data Availability

The data used to support the findings of this study are included within the article.

Conflicts of Interest

The author declares that there are no conflicts of interest regarding the publication of this paper.

References

[1] N. A. Alghamdi and H. M. Youssef, "Dual-phase-lagging thermoelastic damping in-extensional vibration of rotating nano-ring," *Microsystem Technologies*, vol. 23, no. 10, pp. 4333–4343, 2017.

[2] M. A. Biot, "Thermoelasticity and irreversible thermodynamics," *Journal of Applied Physics*, vol. 27, no. 3, pp. 240–253, 1956.

[3] H. M. Youssef and N. A. Alghamdi, "Thermoelastic damping in nanomechanical resonators based on two-temperature generalized thermoelasticity theory," *Journal of Thermal Stresses*, vol. 38, no. 12, pp. 1345–1359, 2015.

[4] H. W. Lord and Y. Shulman, "A generalized dynamical theory of thermoelasticity," *Journal of the Mechanics and Physics of Solids*, vol. 15, 1967.

[5] R. S. Dhaliwal and H. H. Sherief, "Generalized thermoelasticity for anisotropic media," *Quarterly of Applied Mathematics*, vol. 38, no. 1, pp. 1–8, 1980.

[6] C. M. Hoang, "Thermoelastic damping depending on vibration modes of nano beam resonator," *Communications on Physics*, vol. 25, no. 4, p. 317, 2015.

[7] A. K. Naik, M. S. Hanay, W. K. Hiebert, X. L. Feng, and M. L. Roukes, "Towards single-molecule nanomechanical mass spectrometry," *Nature Nanotechnology*, vol. 4, no. 7, pp. 445–450, 2009.

[8] A. D. O'Connell, M. Hofheinz, M. Ansmann et al., "Quantum ground state and single-phonon control of a mechanical resonator," *Nature*, vol. 464, no. 7289, pp. 697–703, 2010.

[9] J. T. M. van Beek and R. Puers, "A review of MEMS oscillators for frequency reference and timing applications," *Journal of Micromechanics and Microengineering*, vol. 22, no. 1, Article ID 13001, 2011.

[10] J. N. Sharma and D. Grover, "Thermoelastic vibrations in micro-/nano-scale beam resonators with voids," *Journal of Sound and Vibration*, vol. 330, no. 12, pp. 2964–2977, 2011.

[11] Y. Sun and M. Saka, "Thermoelastic damping in micro-scale circular plate resonators," *Journal of Sound and Vibration*, vol. 329, no. 3, pp. 328–337, 2010.

[12] N. S. Al-Huniti, M. A. Al-Nimr, and M. Naji, "Dynamic response of a rod due to a moving heat source under the hyperbolic heat conduction model," *Journal of Sound and Vibration*, vol. 242, no. 4, pp. 629–640, 2001.

[13] E. A. N. Al-Lehaibi and H. M. Youssef, "Vibration of gold nano-beam with variable young's modulus due to thermal shock," *World Journal of Nano Science and Engineering*, vol. 05, no. 04, pp. 194–203, 2015.

[14] B. A. Boley, "Approximate analyses of thermally induced vibrations of beams and plates," *Journal of Applied Mechanics*, vol. 39, no. 1, pp. 212–216, 1972.

[15] J. Kidawa-Kukla, "Application of the Green functions to the problem of the thermally induced vibration of a beam," *Journal of Sound and Vibration*, vol. 262, 2003.

[16] G. Manolis and D. Beskos, "Thermally induced vibrations of beam structures," *Computer Methods in Applied Mechanics and Engineering*, vol. 21, 1980.

[17] N. A. Alghamdi, "Dual-phase-lagging thermoelastic damping vibration in micro- nano scale beam resonators with voids," *International Journal of Medical and Clinical Research*, vol. 5, 2017.

[18] M. Javani, Y. Kiani, and M. R. Eslami, "Rapid heating vibrations of FGM annular sector plates," *Engineering with Computers*, vol. 37, no. 1, pp. 305–322, 2021.

[19] H. Ma, S. Yang, H. Wang, N. Li, and F. Jia, "The thermal-structural analysis of a pin under high accelerated stress

screening test," *IEEE Transactions on Components, Packaging, and Manufacturing Technology*, vol. 9, no. 9, pp. 1794–1804, 2019.

[20] M. A. Biot, "Theory of stress-strain relations in anisotropic viscoelasticity and relaxation phenomena," *Journal of Applied Physics*, vol. 25, no. 11, pp. 1385–1391, 1954.

[21] M. A. Biot, "Variational principles in irreversible thermodynamics with application to viscoelasticity," *Physical Review*, vol. 97, no. 6, pp. 1463–1469, 1955.

[22] A. D. Drozdov, "A constitutive model in finite thermo-viscoelasticity based on the concept of transient networks," *Acta Mechanica*, vol. 133, no. 1-4, pp. 13–37, 1999.

[23] M. A. Ezzat and A. S. El-Karamany, "The relaxation effects of the volume properties of viscoelastic material in generalized thermoelasticity," *International Journal of Engineering Science*, vol. 41, 2003.

[24] J. M. Carcione, F. Poletto, and D. Gei, "3-D wave simulation in anelastic media using the Kelvin-Voigt constitutive equation," *Journal of Computational Physics*, vol. 196, no. 1, pp. 282–297, 2004.

[25] D. Grover, "Viscothermoelastic vibrations in micro-scale beam resonators with linearly varying thickness," *Canadian Journal of Physics*, vol. 90, no. 5, pp. 487–496, 2012.

[26] D. Grover, "Damping in thin circular viscothermoelastic plate resonators," *Canadian Journal of Physics*, vol. 93, no. 12, pp. 1597–1605, 2015.

[27] D. Grover, "Transverse vibrations in micro-scale visco-thermoelastic beam resonators," *Archive of Applied Mechanics*, vol. 83, no. 2, pp. 303–314, 2013.

[28] D. Grover and R. K. Seth, "Viscothermoelastic micro-scale beam resonators based on dual-phase lagging model," *Microsystem Technologies*, vol. 24, no. 3, pp. 1667–1672, 2018.

[29] K. S. Novoselov, A. K. Geim, S. V. Morozov et al., "Electric field effect in atomically thin carbon films," *Science*, vol. 306, no. 5696, pp. 666–669, Oct. 2004.

[30] P. N. Nirmalraj, T. Lutz, S. Kumar, G. S. Duesberg, and J. J. Boland, "Nanoscale mapping of electrical resistivity and connectivity in graphene strips and networks," *Nano Letters*, vol. 11, no. 1, pp. 16–22, 2011.

[31] K. Saanouni, J. F. Mariage, A. Cherouat, and P. Lestriez, "Numerical prediction of discontinuous central bursting in axisymmetric forward extrusion by continuum damage mechanics," *Computers & Structures*, vol. 82, no. 27, pp. 2309–2332, 2004.

[32] D. Grover and R. K. Seth, "Generalized viscothermoelasticity theory of dual-phase-lagging model for damping analysis in circular micro-plate resonators," *Mechanics of Time-dependent Materials*, vol. 23, no. 1, pp. 119–132, 2019.

[33] H. M. Youssef, "Vibration of gold nanobeam with variable thermal conductivity: state-space approach," *Applied Nanoscience*, vol. 3, no. 5, pp. 397–407, 2013.

[34] D. Tzou, *Transfer M-tMH the Lagging Behavior*, Taylor & Francis, Washington, 1997.

[35] K. A. Elsibai and H. M. Youssef, "State-Space approach to vibration of gold nano-beam induced by ramp type heating without energy dissipation in femtoseconds scale," *Journal of Thermal Stresses*, vol. 34, no. 3, pp. 244–263, 2011.

[36] A. E. Abouelregal and M. Marin, "The size-dependent thermoelastic vibrations of nanobeams subjected to harmonic excitation and rectified sine wave heating," *Mathematics*, vol. 8, no. 7, p. 1128, 2020.

[37] A. M. H. Yahya, A. E. Abouelregal, K. M. Khalil, and D. Atta, "Thermoelastic responses in rotating nanobeams with variable physical properties due to periodic pulse heating," *Case Studies in Thermal Engineering*, vol. 28, Article ID 101443, 2021.

[38] H. M. Youssef and A. A. El-Bary, "Generalized thermoelastic infinite layer subjected to ramp-type thermal and mechanical loading under three theories-state space approach," *Journal of Thermal Stresses*, vol. 32, no. 12, pp. 1293–1309, 2009.

[39] K. Lotfy, W. Hassan, A. A. El-Bary, and M. A. Kadry, "Response of electromagnetic and Thomson effect of semiconductor medium due to laser pulses and thermal memories during photothermal excitation," *Results in Physics*, vol. 16, Article ID 102877, 2020.

[40] S. M. Abo-Dahab, K. Lotfy, and A. Gohaly, "Rotation and magnetic field effect on surface waves propagation in an elastic layer lying over a generalized thermoelastic diffusive half-space with imperfect boundary," *Mathematical Problems in Engineering*, vol. 2015, Article ID 671783, 15 pages, 2015.